Composites Part B 306 (2025) 112739

Contents lists available at ScienceDirect

Composites Part B

journal homepage: www.elsevier.com/locate/compositesb

Unveiling the anisotropy and mechanism of magnetic alignment of graphene in polymer composites for efficient absorption of THz radiations (0.3–3.0 THz)

Premika Govindaraj [a], Sleeba Varghese [b,c], Anna Sokolova [d], Molong Han [e], Saulius Juodkazis [e,f], Dominique Appadoo [g], Franz Konstantin Fuss [h], Nisa Salim [a], Nishar Hameed [a,*]

[a] School of Engineering, Swinburne University of Technology, Melbourne, Victoria, 3122, Australia
[b] Department of Mathematics, School of Science, Computing and Engineering Technologies, Swinburne University of Technology, Melbourne, Victoria, 3122, Australia
[c] Sorbonne Université, CNRS, Physico-chimie des Électrolytes et Nanosystèmes Interfaciaux, PHENIX, F-75005 Paris, France
[d] Australian Centre for Neutron Scattering, ANSTO, Lucas Heights, New South Wales, 2234, Australia
[e] Optical Sciences Center, Faculty of Science, Engineering and Technology, Swinburne University of Technology, Hawthorn VIC, 3122, Australia
[f] Laser Center, Vilnius University, Sauletekio 10, Vilnius, Lithuania
[g] Australian Synchrotron Company Ltd., Blackburn Road, Clayton, VIC, 3168, Australia
[h] Chair of Biomechanics, Faculty of Engineering Science, University of Bayreuth, Bayreuth, D-95447, Germany

ARTICLE INFO

Keywords:
Graphene
Polyvinyl alcohol
Small angle scattering
THz spectroscopy
Magnetic field
Magnetic alignment

ABSTRACT

Flexible polymer films containing highly aligned graphene flakes were designed using low magnetic field for Terahertz (THz) shielding applications. The alignment of graphene resulted in a unique dark-bright field macroscopic patterns on the cured composite films. On a microscopic scale, the alignment of graphene resulted in a distinctive chain-like structure that favour an effective electron flow path resulting in an electron mobility and optimal electrical conductivity of 7.2 cm^2/Vs and 3.3 x 10^{-7} S/cm, respectively, which is extremely higher than the homogenous composite for the lowest graphene loading of 1 wt%. For the first time, an aligned composite film of 100 μm thickness was characterised using the synchrotron beam in the THz regime – 0.3 to 3.0 THz and exhibited an exceptionally high absorptance of 56.6 % of T-rays for 1 wt% graphene concentration. Simultaneously, the mechanism of orientation and the *in-situ* alignment of graphene in the magnetic field was characterised using the time-of-flight small angle neutron scattering technique and their probability of alignment, anisotropy factor were estimated. The *in-situ* neutron experiments indicate that when the applied magnetic field is perpendicular to the wave vector of the incoming neutron beam, a pronounced anisotropy is observed in the total unpolarized beam due to the alignment of graphene flakes. The exploration of magnetic alignment of graphene and determination of optical anisotropy lays foundation for further discovery of aligned graphene-based composite. The outstanding performance and high efficiency of aligned graphene composites present a huge potential in THz devices, polarization control and shielding solutions for T-rays.

1. Introduction

The promising advancement in materials and scientific methodologies has resulted in the rapid expansion of Terahertz (THz) technology. THz waves are electromagnetic radiations with frequency range of 0.1–1.0 THz, or wavelength range of 0.3–3.0 mm [1]. Because of their intrinsic non-ionising nature, strong absorption by water and coupling to phonon frequencies of solid state materials, quantum/electronic relevance of optical transitions, they show a favourable potential in applications such as medical imaging [2], defence and security [3], communication and sensing for 6G and beyond [4]. The growth of technology has led to the demand for advanced multifunctional materials that are capable to operate and shield the high frequency electromagnetic radiations.

Since the discovery of Graphene, its mechanical, electrical, thermal, and optical properties, have drawn the attention for the advancement of multifunctional composite materials [5]. However, the extensive potential of graphene is not witnessed in composite materials due to the

* Corresponding author.
E-mail address: nisharhameed@swin.edu.au (N. Hameed).

https://doi.org/10.1016/j.compositesb.2025.112739
Received 15 May 2024; Received in revised form 24 April 2025; Accepted 20 June 2025
Available online 26 June 2025

poor dispersion and discontinuous interface of graphene in the matrix [6]. Increasingly graphene in various forms is utilised in electromagnetic interference (EMI) shielding applications due to their excellent electrical properties. Some of the recent studies reported that graphene as a filler in composites exhibited excellent shielding efficiency in the MHz and GHz regions [7–9]. There is only one study that we are aware that tested the shielding efficiency of graphene composites in THz range 0.22–0.35 THz [10].

Herein we report a novel composite made up of aligned graphene in a polymer matrix that have the potential to outperform the current graphene polymer composites in terms of electrical and optical properties. In this study, we have investigated static magnetic field to align graphene in a polymer composite film. The composite exhibited a macroscopic alignment of graphene by presenting dark and bright patterns on the film. The region that appears dark indicate the orientation and attraction of graphene towards magnetic field. Further, the mechanism of graphene alignment under magnetic field is mathematically investigated. The magnetic moment, potential and gravitational energies on the graphene flakes and the probability of graphene alignment at different magnetic fields and temperature is estimated. Further the *in-situ* magnetic alignment of graphene flakes in the polymer dispersion is evaluated using time-of-flight small angle neutron scattering (SANS) and their anisotropy factor is determined. The limitation of graphene agglomeration in the composites is addressed in the present work by aligning graphene flakes inside composite films. The potential improvement in electrical properties and the THz absorption efficiency of aligned polymer composites is presented herein.

2. Experimental

2.1. Preparation of aligned graphene composite films

The graphene used in the current study was synthesised by electrochemical exfoliation of highly oriented pyrolytic graphite (HOPG) (as shown in Fig. 1). A desired amount of graphene as composite fillers was dispersed in water at 0.1, 1, 5 and 15 wt% contents under ultrasonication for 1 h. A calculated quantity of polyvinyl alcohol - PVA (2 wt % and 5 wt%) was added into the graphene dispersions and stirred at 90^{o}C for 3 h to prepare homogenous dispersions. All the composite film samples were prepared using 5 wt% PVA dispersion as 2 wt% PVA samples were not workable. The prepared composite dispersions were cast on a pertri dish in the presence of an external magnetic field (shown in Fig. S2) and dried in the oven at 60^{o}C. The magnetic field was maintained until the solution was completely dried and free-standing aligned graphene/PVA films were obtained. The region above the magnet appeared dark compared to the remaining part of the film. Schematic of the aligned composite film preparation is shown in Fig. 1.

2.2. Characterization

The morphology and the microstructure of samples were examined by field emission scanning electron microscope (SEM). The electrical mobility conductivity of composite films was measured by Van der Pauw method using Ecopia HMS-3000 Hall measurement system. The thickness of the films was measured using 3D profilometer.

The *in-situ* magnetic alignment of graphene in PVA dispersions was studied using neutron scattering. Series of composite solutions were prepared using PVA with concentrations 2, 5 wt% and 1, 5, and 15 wt% GNP by mass with various concentrations of PVA. The dispersions were ultrasonicated for 30 min before SANS measurements, performed using time-of-flight (ToF) – Bilby, small angle neutron scattering beamline at the Australian Centre for Neutron Scattering (ACNS) in ANSTO [11]. Samples were prepared with D_2O as a solvent and measured in 2 mm path-length, in a custom-built temperature-controlled cells. The *in-situ* vertical transverse magnetic field was applied using a 1 T field electromagnet. The ToF instrument Bilby utilises a range of wavelengths from 2 to 20 Å. For the described experiments, the range from 4 Å to 14 Å has been chosen to optimise data quality. Bilby is equipped with two sets of position-sensitive 2D detectors, one square rear and another consisting of four curtains - two vertical and two horizontal detectors. The main detector was located 18 m from the sample, while the front ones were at 5 m (up and down) and 4 m (left and right). The wavevector q range taken for the data analysis was from 0.001 Å^{-1} to 0.2 Å^{-1}. Data at higher q which do not contain structural information has been discarded.

Data reduction was performed using Mantid software suite. The main equation for data reduction is shown below:

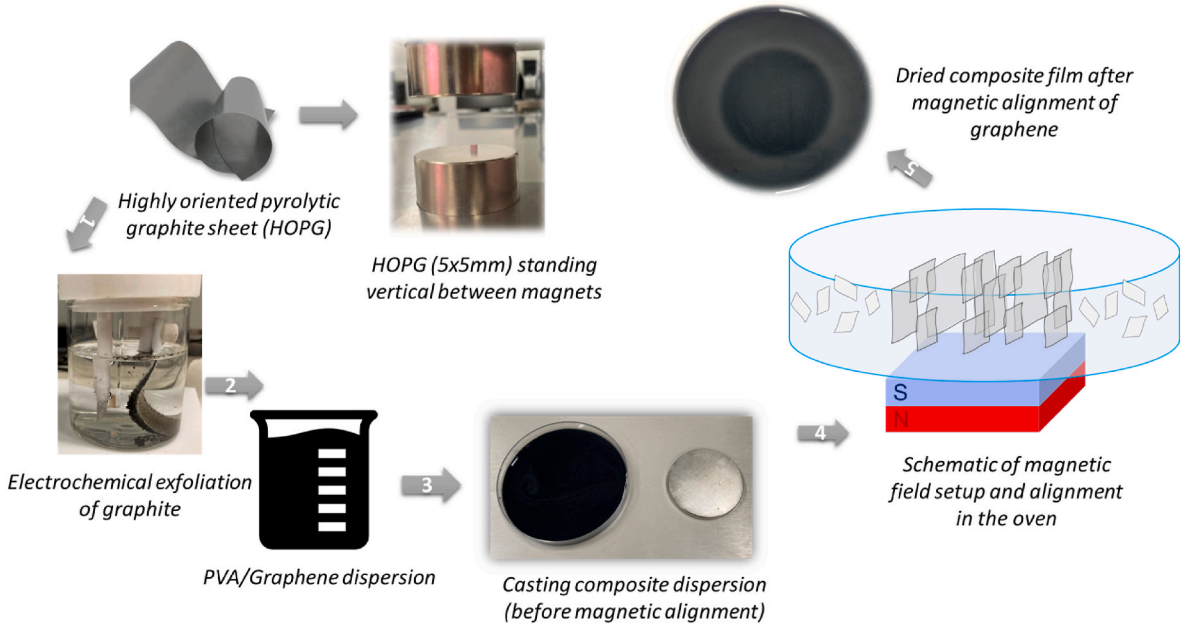

Fig. 1. Schematic showing the preparation of aligned composite graphene films. Graphene micro-sheets align along the magnetic B-field; however, their azimuthal orientation is random.

$$I(Q) = \frac{1}{d_{sam}} \cdot \frac{\sum_{R,\lambda \subset Q} C_{sam,corr}(R,\lambda)}{M \cdot \sum_{R,\lambda \subset Q} T_{corr}(\lambda,R) \cdot \left[\frac{I_{empty\_beam}(\lambda)}{M_{empty\_beam} \cdot att_{empty\_beam}}\right] \cdot \Omega(R) \cdot Det_{flood}(R)}$$

Where $C_{sam,corr}$ is the measured counts per pixel per wavelength, I_{empty_beam} is the intensity of the empty beam collected for M_{empty_beam} time, M is a time measure for the data collection, att_{empty_beam} is attenuation factor, $\Omega(R)$ is the solid angle, Det_{flood} is a detector response function, T_{corr} is the sample transmission, and d_{sam} is the sample thickness.

The raw data is normalized to the transmission, and the background is corrected using a blocked beam measurement. Scaling for absolute intensities was achieved by considering sample thickness and an empty beam measurement. Scattering from the empty cell, D_2O and PVA

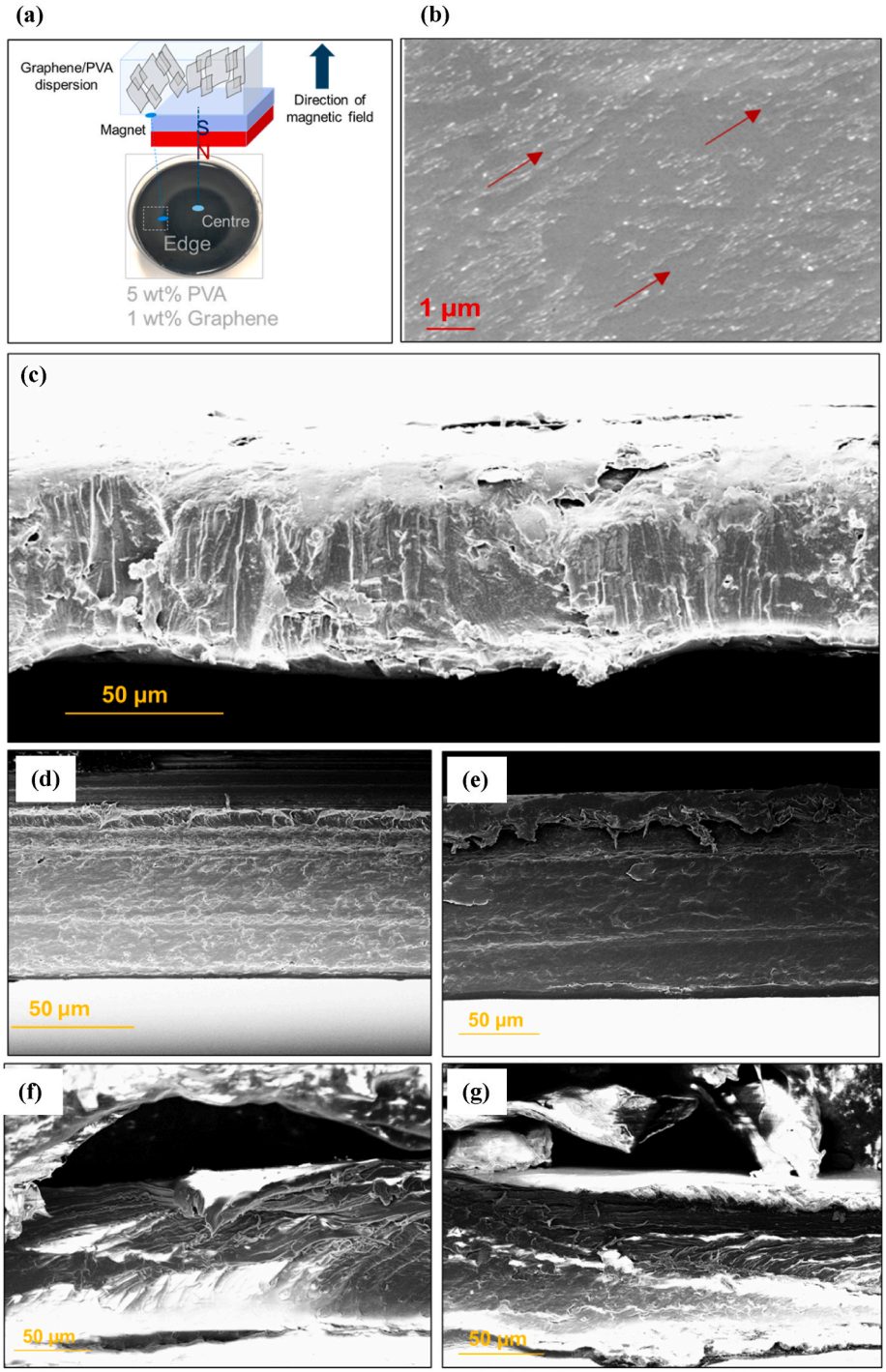

Fig. 2. (a) Schematic showing the orientation of graphene flakes of PVA-Graphene film cured in a static magnetic field. Note: The graphene illustration is purely schematic and does not imply that the flakes are oriented with their normal directions parallel to one another. (b) Alignment of graphene flakes in PVA matrix (Top view). Red arrow on the image show the chain like formations of the graphene due to the magnetic field. Cross-sectional view (c) showing the random distribution of graphene in PVA-Graphene film cured without magnetic field, (d, e) Graphene alignment in PVA-Graphene from center region of the film, (f, g) Graphene orientation in PVA-Graphene film from an edge region of the film. (For interpretation of the references to colour in this figure legend, the reader is referred to the Web version of this article.)

solution is subtracted to obtain the information on graphene. The magnetic alignment of graphene in the dispersions was studied at three different magnetic fields of 0, 0.1, & 1.0 T individually and at three different temperatures of 10, 25 and 80°C.

The optical properties of aligned composites were characterized at the THz Far-IR beamline at the Australian Synchrotron. Near-normal incidence transmission and reflection optics (N^2ITRO, Bruker) technique coupled to a polariser was used to measure the reflection and transmission in the 0.3–3 THz range. A Si bolometer (10–370 cm^{-1}) was used as the detector with a 125 μm Mylar beamsplitter (5–25 cm^{-1}) for the experiments. Polarization is defined as x-pol. and y-pol.in room frame of reference along the direction of propagation (z-axis) in transmission mode. Data analysis was carried out with OPUS 8.0 software (Bruker Optik GmbH).

3. Results and discussion

3.1. Morphology of magnetic field-induced alignment of graphene in PVA/graphene composite films

The alignment of graphene flakes within the PVA films subjected to a magnetic field during curing was studied using SEM. The solution of PVA/Graphene was poured into a Petri dish and placed just above the strong neodymium magnet (0.2 T) and the direction of applied magnetic field is shown in Fig. 2 (a). The magnetic field instantaneously attracted the graphene flakes from the solution towards the magnet forming a dark and bright field. A dark field formed just above the magnet signifying the attraction and orientation of graphene flakes, and a bright field is found away from the magnet, where the orientation of graphene is inhomogeneous. Fig. 2 (b) shows the alignment of graphene flakes in the PVA/Graphene film just above the magnet (termed as 'Center'). The flakes appeared as stripes in the direction of the applied magnetic field under an SEM, which is represented by the red arrows in Fig. 2 (b). Chain-like alignment of graphene flakes extended over the entire composite film in centre region. Although the graphene flakes are not functionalised with any ferromagnetic materials, their response to the application of a magnetic field is due to the intrinsic diamagnetic behaviour of the material. As a result, azimuthal orientation of graphene flakes is expected to be arbitrary, however, they tend to be plane-oriented along the B-field lines. The magnetism of the carbon materials is attributed to the defect-induced mechanism, which arises in the graphene flakes during the electrochemical exfoliation and mechanical forces exerted during the sonication processes. The solution of PVA/Graphene was allowed to cure in the oven in the presence of magnets, and the dried film also exhibited a dark and bright field.

Further, the orientation of graphene flakes was studied by examining the cross-section of the PVA/Graphene composite films. Fig. 2 (c) is the cross-section of PVA/Graphene film without a magnetic field. The flakes of graphene are observed to be randomly distributed and aggregated throughout the PVA matrix.

Fig. 2(d) and (e), show the cross-section of PVA/Graphene film from the center region. The cross-section shows the flat structure or the in-plane of graphene flakes which signifies the flakes are vertically oriented just above the magnet. Compared to the random distribution of graphene in the PVA film, where graphene flakes predominantly aggregate (Fig. 2(c)), the cross-section of the magnetically aligned film exhibits a uniform distribution. Fig. 2(f) and (g), show the cross-sectional morphology of PVA/graphene film from the edge region. The graphene flakes are randomly oriented, showing a mixture of flat (in-plane) and edge (through-plane) structures of the graphene flakes. This shows that, just at the edge of the magnet, flakes are randomly distributed, and they exhibit rotation in the presence of the magnetic field.

In this study, magnetic alignment of graphene flakes was achieved at a relatively low magnetic field of 0.2 T, significantly lower than the field strengths (>10 T) reported in previous studies for aligning carbon nanotubes (CNTs) in polymer matrices such as PET [12] and epoxy [13]. For example, aligning single-walled carbon nanotubes (SWCNTs) in PET matrices has required magnetic fields ranging from 3.0 to 9.4 T, while multi-walled carbon nanotubes (MWCNTs) have been aligned only under much stronger fields of 15–25 T.

This discrepancy can be attributed to fundamental differences in particle properties and matrix interactions. CNTs possess a high aspect ratio and small cross-sectional area, leading to lower magnetic susceptibility anisotropy ($\Delta\chi$), which diminishes the magnetic torque generated per unit volume. In addition, their elongated geometry experiences greater rotational drag in viscous polymer matrices, requiring stronger fields to achieve alignment.

In contrast, graphene flakes, particularly those derived from high-quality HOPG as used in our study, have a larger 2D geometry and higher $\Delta\chi$, which together result in stronger magnetic torque under modest fields. Furthermore, the crystalline nature of HOPG-derived flakes enhances anisotropic response compared to more disordered graphene from graphite powder. The magnetic moments as a function of applied magnetic field measured for HOPG and graphene flakes is shown in Fig. S4.

Thus, the combination of flake morphology, higher intrinsic magnetic anisotropy, and high-quality material enables alignment at much lower magnetic fields than previously reported for nanocarbon systems. This finding not only contrasts with established CNT-based studies but also underscores the importance of graphene source and flake characteristics in enabling low-field alignment — a potentially scalable and energy-efficient route for graphene-based composite processing.

3.2. Mechanism of magnetic field-induced graphene alignment

3.2.1. Derivation for the magnetic moment of a graphene flake in the magnetic field

The intrinsic structural property and the Landau diamagnetic characteristic of the graphene favour the magnetic alignment of graphene [14]. We assume the graphene flakes as a flat structure having π electrons that are free to move in the in-plane direction. The graphene flakes dispersed in the PVA solution are defined with reference to the axes x, y, z. The in-plane axis of the graphene flake remains along the x-y plane, and the through-plane axis is parallel to the z-axis. The schematic of the graphene flakes with respect to the axis is shown in Fig. 3 (a).

The volume magnetic tensor of the surrounding polymeric medium (χ_1) and the graphene flakes (χ_2) is defined as per Equation (1) [15]

$$\chi_1 = \begin{pmatrix} \chi_1 & 0 & 0 \\ 0 & \chi_1 & 0 \\ 0 & 0 & \chi_1 \end{pmatrix}, \chi_2 = \begin{pmatrix} \chi_{2,x} & 0 & 0 \\ 0 & \chi_{2,y} & 0 \\ 0 & 0 & \chi_{2,z} \end{pmatrix} \quad (1)$$

where χ_1 is the isotropic magnetic susceptibility of the polymer solution and the $\chi_{2,x}$, $\chi_{2,y}$, $\chi_{2,z}$ is the anisotropic magnetic susceptibility of graphene flakes. For graphene flakes, the susceptibility along x and y axes remain on the in-plane (x-y plane), hence $\chi_{2,x} = \chi_{2,y} = \chi_{2,\parallel}$ and the susceptibility along z-axis lie along out-of-plane (z-axis), $\chi_{2,z} = \chi_{2,\perp}$.

As shown in Fig. 3 (a), the applied static magnetic field B_0 is at angle θ^* with respect to z-axis and makes a projected angle ϕ with respect to x-axis, along x-y plane. Then the applied magnetic field can be expressed as Equation (2):

$$B_0 = B_0 \left(Sin\,\theta^*\ Cos\,\phi\hat{x} + Sin\,\theta^*\ Sin\,\phi\hat{y} + Cos\,\theta^*\hat{z}\right) \quad (2)$$

where B_0 is the magnetic field amplitude, which is expected to be uniform over the graphene micro flakes. The submerged graphene flakes experience an induced magnetic moment in the presence of an applied static magnetic field, which tends to rotate the graphene particles. The induced magnetic moment (m_{eff}) is expressed as Equation (3) [16]:

$$m_{eff} = \frac{V}{\mu_0}\left(\chi_2 - \chi_1\right).B_{in} \quad (3)$$

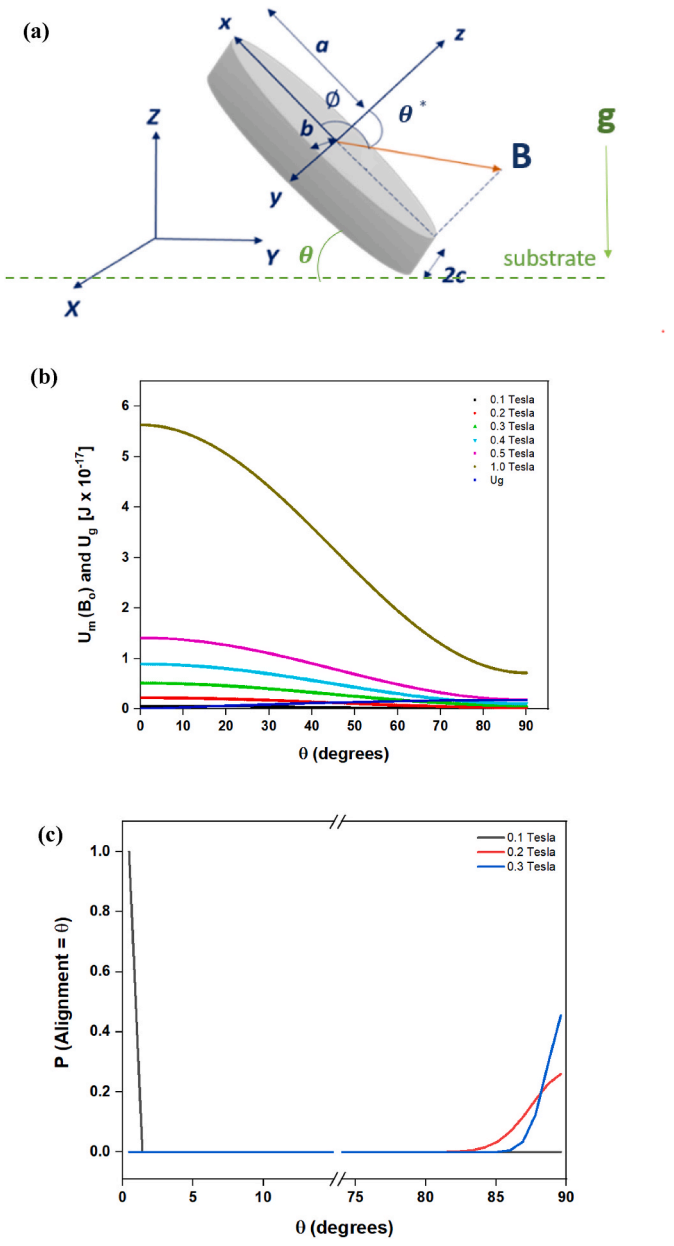

Fig. 3. (a) Schematic representation of graphene flake with respect to the x, y, and z axis. (b) Magnetic and gravitational energies of graphene flakes vs angle with respect to the substrate for different magnetic fields. As the magnetic field increases, the energy landscape is dominated by magnetic energies which indicate out-of-plane orientation of graphene flakes. (c) Probability of graphene flakes to be in different orientational angles under different magnetic fields at 10°C.

where μ_0 is the permeability of free space, V is the volume of the graphene flake and B_{in} is the magnetic field inside a graphene flake, with reference to the x,y,z planes are given by $B_{in,k}$ $(k = x,y,z)$ in Equation (4):

$$B_{in,k} = \frac{\mu_1}{\mu_1 + (\mu_{2,k} - \mu_1)\, L_k} B_{0,k} \quad 4$$

Here the $\mu_{2,k} = 1 + \chi_{2,k}$ and μ_1 are the relative permeability of graphene flake and the surrounding polymer solution respectively. $B_{0,k}$ is the component of applied magnetic field and L_k $(0 \le L_k \le 1)$ is the demagnetisation factor that account for particle geometry and magnetisation. For a diamagnetic particle like graphene (without any coating), the susceptibility $\chi < 0$, and the volume susceptibilities are negligibly small $(|\chi| < 10^{-4})$. Hence the denominator $(\mu_{2,k} - \mu_1)\, L_k = (\chi_{2,k} - \chi_1)\, L_k \ll \mu_1$, and we can assume $B_{in,k} \approx B_{0,k}$, which means the demagnetising field inside a diamagnetic particle is extremely small. Hence the effective induced magnetic moment on a diamagnetic particle such as graphene flake is independent of particle geometry and shape and is expressed as Equation (5):

$$m_{eff} \approx \frac{V}{\mu_0} (\chi_2 - \chi_1)\, B_0 \quad 5$$

In this study, the induced magnetic moment of graphene flakes is modelled as a function of their magnetic susceptibility anisotropy ($\Delta\chi$) and the strength of the externally applied magnetic field. For thin, high-aspect-ratio graphene flakes derived from HOPG, the demagnetising field is negligible due to their planar geometry and minimal thickness. As a result, the internal magnetic field within the flake is effectively equal to the applied magnetic field, allowing us to approximate the induced magnetic moment as independent of particle geometry in this specific context.

However, while the magnetic torque experienced by a flake may not strongly depend on its size or shape under this approximation, the dynamics of alignment are influenced by both geometry and matrix viscosity. Larger flakes are subject to greater rotational drag, and their motion through a viscous polymer matrix is more hindered than that of smaller flakes. This affects the rate of alignment, even if the thermodynamic tendency to align (driven by magnetic torque) remains the same. However, Erb et al. has confirmed that an increase in viscosity of polymer solutions and resins only slow down the orientation process but does not change the minimum magnetic field required for alignment [17].

3.2.2. *Calculation of magnetic and gravitational potential energies of graphene flakes*

The orientation of graphene flakes with respect to the applied external magnetic field will affect the magnetic and gravitation potential energies U_m and U_g respectively. The graphene flakes are modelled as an ellipsoid disc with half sizes a, b and c. The SEM images of exfoliated graphene flakes (Fig. S5) were used to determine the dimensions. The calculated volume of all graphene flakes *(2πabc)* is determined with the average dimensions (full sizes) being approximately 2.2 μm × 2.5 μm x 65 nm. The magnetic potential energy, U_m, of graphene flakes in a magnetic field is expressed as Equation (6) [15]:

$$U_m = -\int_0^{B_0} m_{eff}(B).\, dB = -\frac{VB_0^2}{2\mu_o}\left[(\chi_{2,\parallel} - \chi_1) + (\chi_{2,\perp} - \chi_{2,\parallel}) Cos^2\,\theta\right] \quad 6$$

To reduce the magnetic potential energy, the graphene tends to rotate until its in-plane direction is parallel to the external magnetic field (i.e $\theta = 90^o$). Thus, the rotation of flakes results in-plane of graphene flakes' lie parallel to the magnetic field, which is also confirmed through the SEM image from the center region. Hence, the magnetic potential energy of graphene flakes is minimum at $\theta = 90^o$ and maximum at $\theta = 0^o$ (as shown in Fig. 3 (b)).

The graphene flakes suspended in the PVA solution also experience gravitational energy which affects their orientation. The gravitational energy of the graphene flake is expressed as Equation (7) [17]:

$$U_g = V(\rho_p - \rho_f)\, gb \sin\theta \quad 7$$

where ρ_p and ρ_f are the densities of graphene and polymer respectively. V is the volume of graphene flake (assumed as ellipsoidal geometry), θ represents the angle between the in-plane direction of the graphene flake and the horizontal plane (as shown in Fig. 3 (a)) and g is the gravity constant. Similar to the magnetic potential energy, gravitational energy

also depends on the orientation of the graphene flakes with respect to the horizontal surface. The gravitational energy is zero when the in-plane axis of graphene lies parallel to the horizontal surface (i.e. $\theta = 0^o$) and maximum when flakes are oriented vertically (i.e. $\theta = 90^o$) (as shown in Fig. 3 (b)). As the magnetic field increases from 0.1 to 1 T, the magnetic potential energy becomes dominant which signifies the out-of-plane alignment.

The overall orientation angle of graphene flakes is governed by the magnetic and gravitational energies of the system. The parameters in Equations (6) and (7) are derived from experimental results as well as literature: $2a = 65$ nm, $2b = 2.2$ μm, $\rho_p = 2.267$ g/cm^3, $\rho_f = 1.269$ g/cm^3, $\rho_p - \rho_f = 2.267\text{-}1.269 = 0.998$ g/cm^3, $\chi_1 = -9 \times 10^{-6}$, $\chi_{2,\|} = -8.2 \times 10^{-5}$, $\chi_{2,\|} = -5.8 \times 10^{-4}$.

3.2.3. Calculation of probability of alignment of the graphene flakes

The orientation preference of graphene flakes at a specific magnetic field strength was studied using Boltzmann statistics. The total energy is assumed to follow the Boltzmann distribution, with the Boltzmann factor at each possible orientation ($0° < \theta < 90°$) expressed as per Equation (8) [18]:

$$e^{\left[-U_m(B_0,\theta)-U_g(\theta)\right]/k_BT} \quad 8$$

where k_B is the Boltzmann constant and T is the absolute temperature. Hence the probability of a graphene flake oriented at an angle θ, ranging from 0° to 90°, is expressed as Equation (9):

$$P_{\theta_1}^{\theta_2} = \int_{\theta_2}^{\theta_1} e^{\frac{\left[U_m(\theta)-U_g(\theta)\right]}{k_BT}} \Big/ Z \quad 9$$

$$Z = \int_{0^o}^{90^o} e^{\left[-U_m(\theta)-U_g(\theta)\right]/k_BT}\, d\theta$$

In Equation (9), Z is the partition function, which is the sum of all Boltzmann factor of all possible states of orientation. From Fig. 3 (c), we can determine the magnetic field required to achieve a particular orientation angle at a temperature of 10 °C. The probability that a graphene flake will be oriented from 89° to 90° at 0.3 T is estimated to be 0.45. We also investigated the orientation preference of graphene flakes at 25 and 80 °C (Fig. S3), and we do not observe any significant variation due to the change in the temperature. The temperature of the

3.3. SANS study

The diamagnetic graphene flakes are suspended in PVA solution, a non-magnetic carrier liquid. On applying magnetic field, the in-plane axis of graphene flakes orients in the direction of the applied field, resulting in vertical orientation of the graphene flakes. Our experiments were carried out in ToF-Bilby SANS beamline coupled with an electromagnet, which provides a static magnetic field up to 1T. A titanium sample holder with a provision for temperature control was used to control the sample temperature. This set-up allows to investigate magnetic field induced orientation of graphene flakes in PVA solution. Fig. 4 (a) depicts the schematics of experimental setup. Through the evacuated flight path, the incoming neutron beam is collimated by set of apertures on to the sample solution (different concentration of graphene dispersed in PVA) placed vertically between the horizontal magnetic field. The assembly of magnetic field and the sample holder position are shown in Fig. 4(b) and (c). The applied filed is perpendicular to the wave vector k_0 of the incoming neutron beam. The scattering vector q is defined as Equation (10):

$$q = k_1 - k_0 = \left(\frac{4\pi}{\lambda}\right) Sin(\psi/2) \quad 10$$

where k_0 and k_1 are the wavevectors of the incident and scattered neutron, respectively, ψ is the scattering angle and λ is the wavelength.

The azimuthal angle θ, specifies the orientation of scattering vector q on the detector. The scattering vector is expressed in terms of ψ and θ as per Equation (11):

$$q = \begin{pmatrix} q_x \\ q_y \\ q_z \end{pmatrix} = q \begin{pmatrix} -\sin\left(\frac{\psi}{2}\right)\cos\left(\frac{\psi}{2}\right)\sin\theta \\ \\ \cos\left(\frac{\psi}{2}\right)\cos\theta \end{pmatrix} = k_o \begin{pmatrix} \cos\psi - 1 \\ \sin\psi\sin\theta \\ \sin\psi\cos\theta \end{pmatrix} \quad 11$$

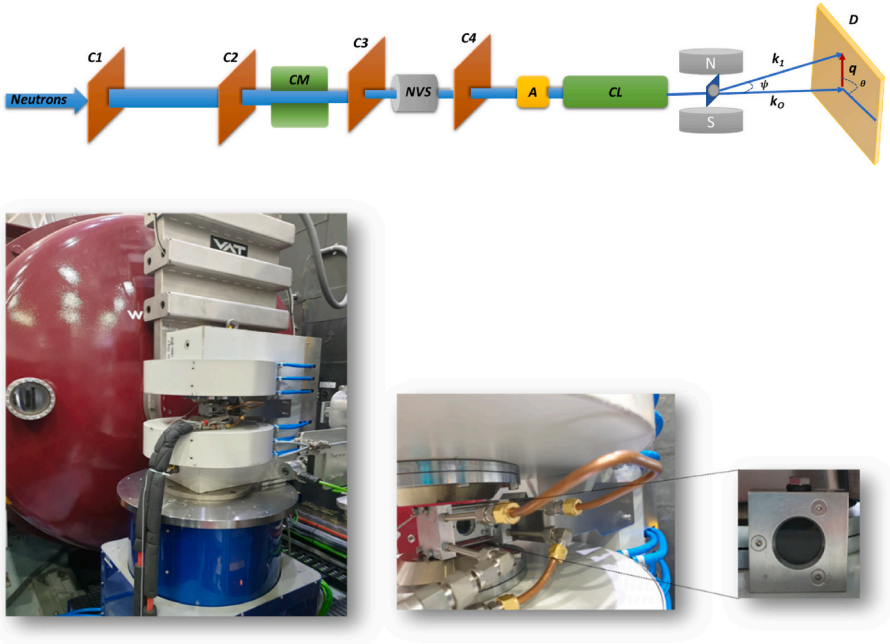

Fig. 4. (a) Schematic representation of experimental set-up (C1 – C4 – chopper systems, CM -wavelength cut-off mirror, NVS – Neutron velocity selector, A – Attenuators, CL – Collimation vessel, NS – Magnetic field, D- Detector panel) (b) Sample area showing the horizontal field magnet (c) Sample positioned vertically in the magnetic field (Inset shows the sample holder containing the PVA/G solution).

3.3.1. In-situ SANS analysis to study the effect of temperature on the graphene flakes orientation under a magnetic field

In our experiments, the external magnetic field is perpendicular to the wave vector k_0 of the incoming neutron beam where $k_0 \parallel e_x$, $H_o \parallel e_z$ (as shown in Fig. 5 (a)), then the scattering vector in Equation: 11 can be approximated as:

$$q = \begin{pmatrix} 0 \\ q_y \\ q_z \end{pmatrix} = q \begin{pmatrix} 0 \\ \sin\theta \\ \cos\theta \end{pmatrix} \quad 12$$

As per the above Equation: 12, the scattering vector is resolved into two components q_y, q_z and their intensities are plotted as $I\left(q_y\right)$ vs q and

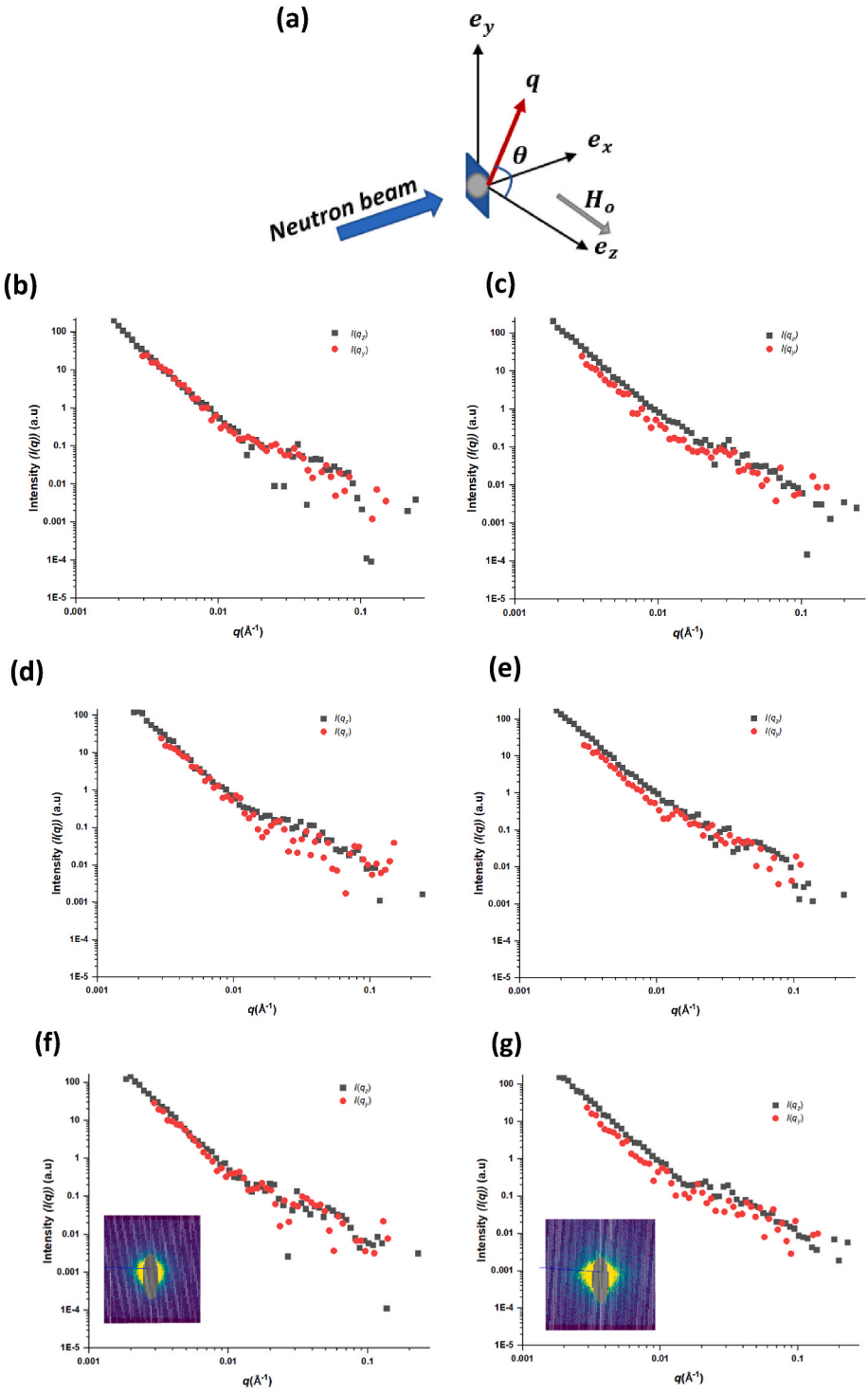

Fig. 5. (a) Schematics of scattering geometry employed in SANS experiment with magnetic field: $k_o \perp H_o$. Scattering data collected from PVA/graphene dispersion at various temperature (T) and magnetic field strength (B). (b) T: 10°C and B: 0 T, (c) T: 10°C and B: 0.1 T, (d) T: 25°C and B: 0 T, (e) T: 25°C and B: 0.1 T, (f) T: 80°C and B: 0 T, (g) T: 80°C and B: 0.1 T Inset image in (f) and (g) shows the evolution of anisotropic 2D scattering pattern (direct beam area is masked) on applying magnetic field. Data is plotted for the sample PVA/Graphene(5 wt%: 1 wt%) dispersed in D_2O.

$I(q_z)$ vs q. In the absence of the magnetic field, the intensities of q_y and q_z remain the same in the low q region (<0.01 $Å^{-1}$, as shown in Fig. 5(b)–(d) and (f). On applying a magnetic field of 0.1 T, the graphene flakes dispersed in PVA solution tends to orient resulting in the variation of intensities $I\left(q_y\right)$ and $I(q_z)$ at the lower q region, clearly illustrating the anisotropy with the magnetic field (as shown in Fig. 5(c)–(e) and (g)). The 2D SANS scattering pattern changes from isotropic, circular shape in the absence of magnetic field to horizontally elongated pattern on applying magnetic field. This indicates the transition of graphene flakes from random distribution to oriented state. The elongation of the scattering cross section in the magnetic field direction indicates the preferred orientation of graphene flakes perpendicular to the applied field. As visible on the inserts of Fig. 5 (f) and (g) (row data detector image), the gravity causes the direct beam profile to become elongated. Appropriate masking was performed during the data reduction to reduce these effects on the reduced data. Although there is obvious variation in the scattering intensities, they remain hardly affected due to the temperatures at 10, 25 and 80 °C. The temperature was chosen in the range between 10 and 80 °C, to avoid the effect of crystallization or degradation of PVA.

To further quantify the scattering anisotropy, the scattering anisotropy factor is determined as per the Equation: 13 [19]:

$$A(q) = \frac{I(q_z) - I\left(q_y\right)}{I(q_z) + I\left(q_y\right)} \quad 13$$

$A(q) = 0$, indicates an isotropic orientation and $A(q) = 1$, indicates complete alignment where the major axis is perpendicular to the applied magnetic field. Table S1 shows the scattering data for q < 0.01 $Å^{-1}$, and the scattering anisotropic factor at different temperatures. It is estimated to be 0.44 ± 0.11, 0.43 ± 0.06 and 0.43 ± 0.06 at 10, 25 and 80°C, respectively. For the temperature range under the study, the $A(q)$ is almost same, suggesting a temperature independent effect on the alignment of graphene flakes in PVA solution. SANS results also support the calculation of probability of alignment of the graphene flakes at different temperatures (Fig. 3 (c) and S3) discussed in section 3.2.3.

3.3.2. *In-situ SANS analysis to study the effect of graphene concentration on the graphene flakes orientation using magnetic field*

The effect of graphene concentration in the orientation of flakes were studied at 3 different concentrations – 1, 5 and 15 wt%. On applying external magnetic field of 0.1 T, irrespective of graphene concentration, the graphene flakes oriented. This is observed as varying scattering intensities $I(q_y)$ and $I(q_z)$ shown in Fig. 6. Table S2 shows the scattering data for $q < 0.01\ A^{0^{-1}}$, and the scattering anisotropic factor at different graphene concentrations. The anisotropy factor is estimated to be 0.41 ± 0.08, 0.65 ± 0.04 and 0.70 ± 0.08 for graphene loadings of 1, 5 and 15 wt% respectively. The increase in the anisotropy factor with the increase in graphene loading is attributed to orientation and accumulation of many graphene flakes. Further graphene flakes are highly polydisperse system with large lateral size (as observed in Fig. S5) which result in folded, crumpled and aggregated structures in the polymer matrix. At higher concentration, the aggregated filler morphology consisting of multiple layers of graphene flakes and the local structures of graphene flakes in the polymer matrix also contribute the increase in anisotropy factor.

3.4. *Electrical conductivity and the Hall effect study*

The in-plane electrical conductivity of graphene flakes is reported to be 10^5 S/cm which is significantly higher than the through-plane electrical conductivity of 1 S/cm [20]. Thus, the anisotropy induced due to magnetic field alignment was estimated to considerably increase the electrical conductivity of PVA-graphene films in the alignment direction. The effect of graphene concentration and the alignment of graphene flakes on the electrical conductivity of the PVA-graphene films are presented in Fig. 7. For comparison, the electrical conductivity of randomly distributed PVA-graphene films is also included in Fig. 7. The results demonstrate that the electrical conductivity of PVA-graphene significantly increased after magnetic alignment compared to the randomly distributed PVA-graphene films. Thus, in magnetically aligned samples due to the chain formation of the graphene flakes along the magnetic lines of force, the mobility of electrons through the composite films are enhanced and more conducting channels are available for electron flow. Under this circumstance, the electrical conductivity of the PVA-graphene films is dominated by tunnelling mechanism.

Further, to confirm the mechanism of electrical conductivity, Hall effect measurements were performed to measure the electron mobility (μ) and carrier concentration (n). At room temperature, for a filler content of 15 wt%, the electrical conductivity of aligned PVA-graphene film is 1.78 x 10^{-5} S/cm and for randomly distribute PVA-graphene film is 2.82 x 10^{-7} S/cm was observed. These values confirm the electrical

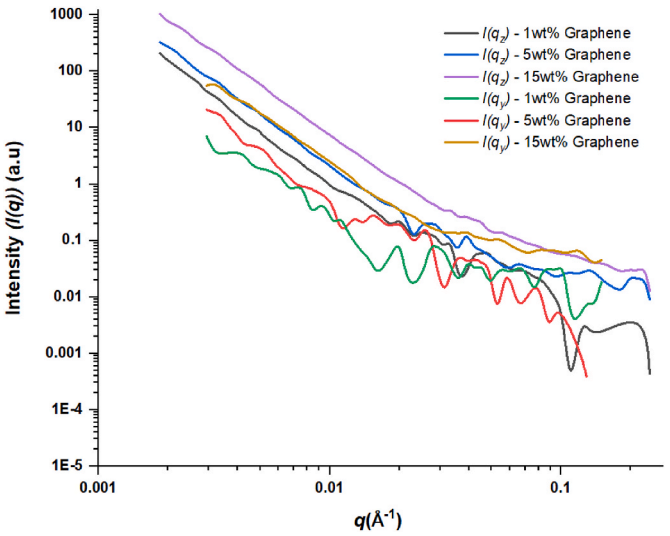

Fig. 6. Scattering data collected from PVA/Graphene dispersion at different concentrations of graphene 1, 5 and 15 wt% on applying 0.1 T external magnetic field and at 25 °C. $I(q_y)$ – Intensity of scattering vector along y-axis and $I(q_z)$ – Intensity of scattering vector along z-axis.

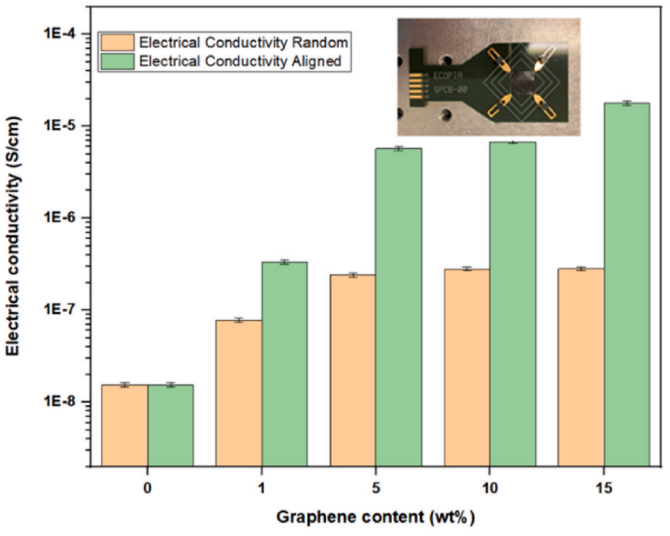

Fig. 7. Effect of graphene content and alignment on the electrical conductivity of PVA/graphene composite films.

conductivity of aligned films is higher by two orders of magnitude of electrical conductivity of randomly distributed PVA-graphene films, thus exhibiting semiconducting nature. The conducting behaviour of an electronic device rely on the mobility of the electrons. The electrical conductivity of the aligned composites is two orders of magnitude higher than the randomly distributed composites, which is consistent with the literature [20]. Wu et al. demonstrated that aligning graphene within an epoxy matrix using an electric field resulted in conductivities 2–3 orders of magnitude higher along the alignment direction compared to both the transverse direction and composites with randomly oriented graphene.

The electrical conductivity depends either on the less number of electrons with high mobility or more number of electrons with lower mobility [21]. Thus, with the increase in graphene concentration from 5 to 15 wt%, the mobility increases from 10^{-1} to 10 cm^2/Vs in a randomly distributed graphene film and from 10 to 10^2 cm^2/Vs in an aligned graphene film. Further, the values of carrier concentration are listed in Table 1. The values of μ and n with the addition of graphene are consistent with the electrical conductivity of the composite films. The carrier concentration values of graphene films increase with graphene concentration, alignment of graphene and changes to negative value. Thus, the results indicate that with the addition of graphene the composite film behave as an n-type semiconductor, which is consistent with previous Hall-effect studies on the composite films [21]. The charge carrier density does exhibit a dependence on graphene content. The increase in magnitude of n (more negative) with graphene content suggests enhanced charge carrier density, but the negative sign might reflect the dominance of electrons (n-type behavior). Further, it can be concluded that alignment of graphene using magnetic field aided in enhanced mobility and more conducting channels compared to randomly distributed composite films with many insulating gaps and poor dispersion.

3.5. Optical properties

3.5.1. Polarization of Australian synchrotron THz radiation using N^2ITRO unit

The synchrotron radiation for THz beamline was extracted from the edge of a dipole magnet using a mirror with 3 mm slit as shown in Fig. 8. With reference to the orbital plane of electron, the radiation from dipole moment is horizontal and vertical polarized. The horizontally polarized radiation is referred to as σ – polarization mode radiation. The vertically polarized radiation is known as π – polarization mode radiation. A combination of σ and π polarization modes results in elliptically polarized radiation above and below the deflection plane of the electron beam.

Polarization of the synchrotron radiation for THz beamline was carried out at the THz/Far-IR beamline in Australian Synchrotron. The elliptically polarised radiation arising from the 3 mm mirror slit can be resolved into circular polarised (E_I – isotropic component) and linear polarised (E_L – aligned along the horizontal slits). A standard stretched polyethylene film polariser was placed normal to the incident beam, and its polarisations was selected by rotating a motorised stage prior to measuring the transmission spectrum. The spectra were measured using a Si bolometer detector and Mylar 125 μm beamsplitter from 10 to 100 cm^{-1}. The intensity in transmission and reflection of the synchrotron beam (without sample) using N^2ITRO setup was measured at four orientation angles of polarizer (is shown in Fig. 9(a) and (b)). Angular dependence of narrow THz radiation using the beamsplitter Mylar 125 μm measured in transmission mode is shown in Fig. 9 (c). Angular measurements were carried out at $\Delta\theta = 15^\circ$ steps in $\theta = 0 - \pi$ range and repeated to complete 2 π polar plot.

Fig. 10 (a) shows the angular dependence of transmission spectra measured at angular orientation steps of every 15°. Using the horizontal and vertical polarised components, the transmitted intensity is established at two angles $\theta = 0$ and $\theta = \pi/2$ as Equation (14) [22].

$$\begin{aligned} E_\theta &= E_0^2\, Cos^2(\theta) + E_{\pi/2}^2\, Sin^2(\theta) \\ &= \left(\frac{1}{2}E_I^2 + E_L^2\right) Cos^2(\theta) + \frac{1}{2}E_I^2\, Sin^2(\theta) \\ &= \left(\frac{1}{2}E_I^2 + E_L^2\right) + \frac{1}{2}E_L^2\, Cos(2\theta) \end{aligned} \quad (14)$$

where $I_{off} = \left(\frac{1}{2}E_I^2 + E_L^2\right)$ is the offset intensity and $I_{amp} = \left(\frac{1}{2}E_L^2\right)$ is the amplitude of intensity transmitted through the analyser. The angular dependence of the spectrum is shown in Fig. 10 (b) and the map is represented as intensity of spectrum in x-axis and the orientation angle in y-axis.

The percentage of linear polarization in the entire spectrum is estimated using Equation (15) [22].

$$Lin = \frac{E_L^2}{E_I^2 + E_L^2} = \frac{I_{amp}}{I_{off}} \quad (15)$$

Polarised radiation was estimated to be a composition of linear ~ 22 % and circular 78 % polarisations due to contributions of the dipole and edge radiations as determined earlier for this THz beamline for broad spectral range [22]. However, this ratio was wavelength dependent and here, we carried out polarization analysis for the lowest wavenumbers 10–100 cm^{-1}. It is evident from Fig. 10 (b) that more linear polarization was at 10–40 cm^{-1} while it was close to circular at around 100 cm^{-1}.

3.5.2. Optical properties of PVA and aligned PVA-graphene composite film measured using N^2ITRO unit

To determine the optical properties of PVA and PVA-Graphene composites, measurement of reflected and transmitted intensities I_R and I_T, respectively, was made from exactly the same position of the microfilm. Measurements of transmittance $T = \frac{I_T}{I_0}$ and reflectance $R = \frac{I_R}{I_0}$ were performed on the same spot on the composite film at a selected polarization angle θ, I_0 is the intensity of the incident THz beam. The absorbance of the THz radiation by the composite films is estimated using energy conservation (Equation: 16):

$$A = 1 - R - T \quad (16)$$

The optical density of the composite film was expressed in terms of A, R and T as per Equations (17) and (18).

$$T = (1 - R) * 10^{-OD} \quad (17)$$

$$A = (1 - R) * \left(1 - 10^{-OD}\right) \quad (18)$$

The absorption of radiation is expressed in terms of absorption coefficient α (cm^{-1}) and the thickness of film d as per Equation (19):

$$\alpha d = \ln(10) OD = 2.303\, OD \quad (19)$$

Table 1
Values of electron mobility (μ) and carrier concentration (n) of PVA/graphene composites at different filler concentrations. The uncertainty in mobility values is estimated to be within ±10 %, determined from multiple sample measurements under identical conditions.

Graphene Distribution	Random					Aligned			
Filler concentration (wt%)	0	1	5	10	15	1	5	10	15
μ (cm^2/Vs)	1.18E-02	0.02E-01	1.90E-01	1.48E+00	1.47E+00	0.72E+01	1.02E+01	9.15E+02	1.01E+02
N (cm^{-3})	8.17E+10	−0.18E+11	−7.95E+11	−0.94E+12	−1.19E+12	−0.21E+11	−6.43E+11	−0.73E+12	−1.10E+12

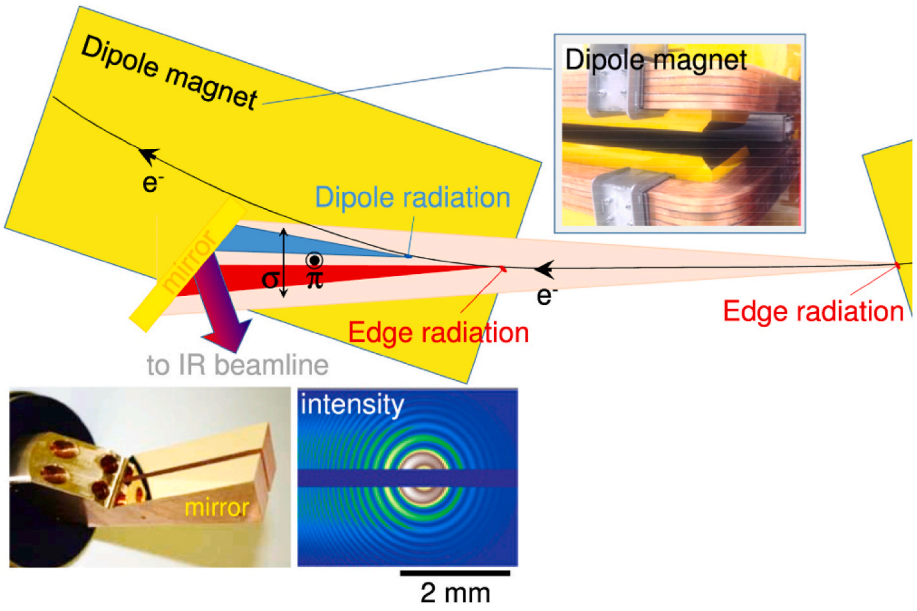

Fig. 8. Schematic showing the generation of synchrotron radiation. The dipole and edge radiation from the source have both σ and π components. The intensity plot shows the distribution of THz radiation at first mirror reflection. (Adopted from Ref. [22]).

The absorption of radiation by the films is regarded as strong when $\alpha d > 1$.

Fig. 11 shows the estimated optical density of PVA (5 wt%) and PVA-Graphene (1 wt%) composite film prepared without the applying magnetic field (B = 0). The Mylar 125 μm beamsplitter exhibits strong interference in the low intensity region, hence, strong artefacts were observed in transmittance $T(\tilde{\nu})$ and reflectance $R(\tilde{\nu})$ spectra. The overall trend of *OD* with respect to wavenumber $\tilde{\nu}$ ($\alpha\, {}^{1}/_{\lambda}$ where λ is the wavelength) was increasing for both PVA and PVA/Graphene composite films. The less explored region at 0.1–1.0 mm wavelengths was selected for *OD* calculations. Usually, a Globar source is used in FTIR spectrometers for the measurements at wavelengths larger than $\tilde{\nu} > 400$ c m^{-1}.

For pristine PVA microfilm, at $\tilde{\nu} > 40$ cm^{-1} ($\lambda = 250$ μm and $\nu = 1{\cdot}2$ *THz*), $OD = 0.3$ and $10^{-0.3} = 0.5$ or half of the intensity passes through the PVA film (shown in Fig. 11 (a)). For the same thickness PVA-Graphene composite film, *OD* was estimated 0.87 and $10^{-0.87} = 0.13$ or only 13 % of the incident THz radiation was transmitted (shown in Fig. 11 (b)). The difference in transmission of incident THz radiation by the films is attributed to absorption of THz radiation by the graphene in the composite film. The slope = 1 (the dashed line shown in the plot) trend of $OD(\tilde{\nu})$ dependence is indicative of this sub-wavelength nature. As ${}^{d}/_{\lambda} \rightarrow 1$, strong absorption was observed in composite films ($OD \rightarrow 1$). Once $\alpha d > 1$, transmitted portion of light becomes small $T \rightarrow 0$ and noise is dominating in the spectral portion of *OD*.

Fig. 12, shows the absorption performance of PVA-Graphene composite film made on magnet B = 0.2 T. The appearance in the visible spectrum clearly showed a difference in the alignment of graphene flakes. As discussed previously in the mechanism of graphene alignment, graphene being diamagnetic is expected to orient the flakes along the B-field lines and at B = 0.2 Telsa, the probability of graphene flakes oriented (θ = 80 to 90°) is greater than zero. The edge region is expected to have the most in-homogenous distribution of graphene in terms of the orientation angle (as shown in the schematics in Fig. 12 (a)). The absorption of radiation by the composite film at the edge region is close to that of PVA with $OD \approx 0.3$. The reflectance was lowest $R \approx 1\%$ across all spectral window in the edge region. Lower reflectance R contributes to higher absorptance $A = (1 - R)\ \left(1 - 10^{-OD}\right)$, with R ≈ 10 % (center) and 0.2 % (edge) at $\tilde{\nu} = 40$ cm^{-1} for the OD = 0.43 (center) and 0.3 (edge)the absorptance A = 56.6 % (center) and 49.8 % (edge).

The orientation of graphene flakes within the PVA–graphene films has contributed to enhanced absorption of THz radiation. Fig. 12(d) presents the absorptance at the center and edge regions of composite films with varying filler loadings. It is evident that the aligned regions exhibit higher absorptance compared to non-aligned areas. Notably, the difference in absorptance between the edge and center is most pronounced at 1 wt% graphene concentration, suggesting a higher degree of orientation at this loading. As the concentration increases, the effectiveness of alignment decreases, likely due to increased flake interactions and aggregation, making it difficult to achieve uniform alignment even under a static magnetic field of 0.2 T. This is reflected in the nearly overlapping error bars for the center and edge regions at 5 wt % and 15 wt%, indicating minimal differences in absorptance due to reduced alignment at higher concentrations.

The diamagnetic nature of graphene flakes makes them plane-aligned along B-field lines, however, their azimuthal orientation perpendicular to the B-lines is arbitrary. Such alignment favors interconnectivity of the graphene network, which is consistent with electrical percolation and increased electrical conductivity. The orientation of electrically conductive graphene plates makes them preferentially oriented perpendicularly out-of-plane (graphene's plane) with respect to the incident linearly polarised electric E-field. This corresponds to the π-polarization (σ-polarization would be aligned with the plane of the flake). Reflection coefficient for the π-pol. $R_\pi < R_\sigma$, which cause stronger absorption losses. Another possible contribution to the absorption of THz E-field is due to the near-field localisation of THz light at the sub-wavelength regions of reduced refractive index, i.e., at the graphene flakes. Such phenomenon was used for 3D modification of dielectrics with ultra-short laser pulses [23]. Once THz E-field is localised on graphene flakes the induced electrical currents contribute to the losses proportionally to the imaginary part of the permittivity $\varepsilon^* = \varepsilon_1 - i(4\pi\sigma/\omega)$, where σ is the conductivity and $\omega = 2\pi c/\lambda$ is the cyclic frequency of light. Indeed, the larger conductivity and lower frequency (e.g., THz) favour a larger imaginary part of the permittivity, hence, larger optical losses.

The present study reveals an optimum absorption of THz radiation using low magnetic field and low graphene concentrations. To further enhance the absorption properties, it is recommended to tailor the charge density of the graphene via doping and defect engineering.

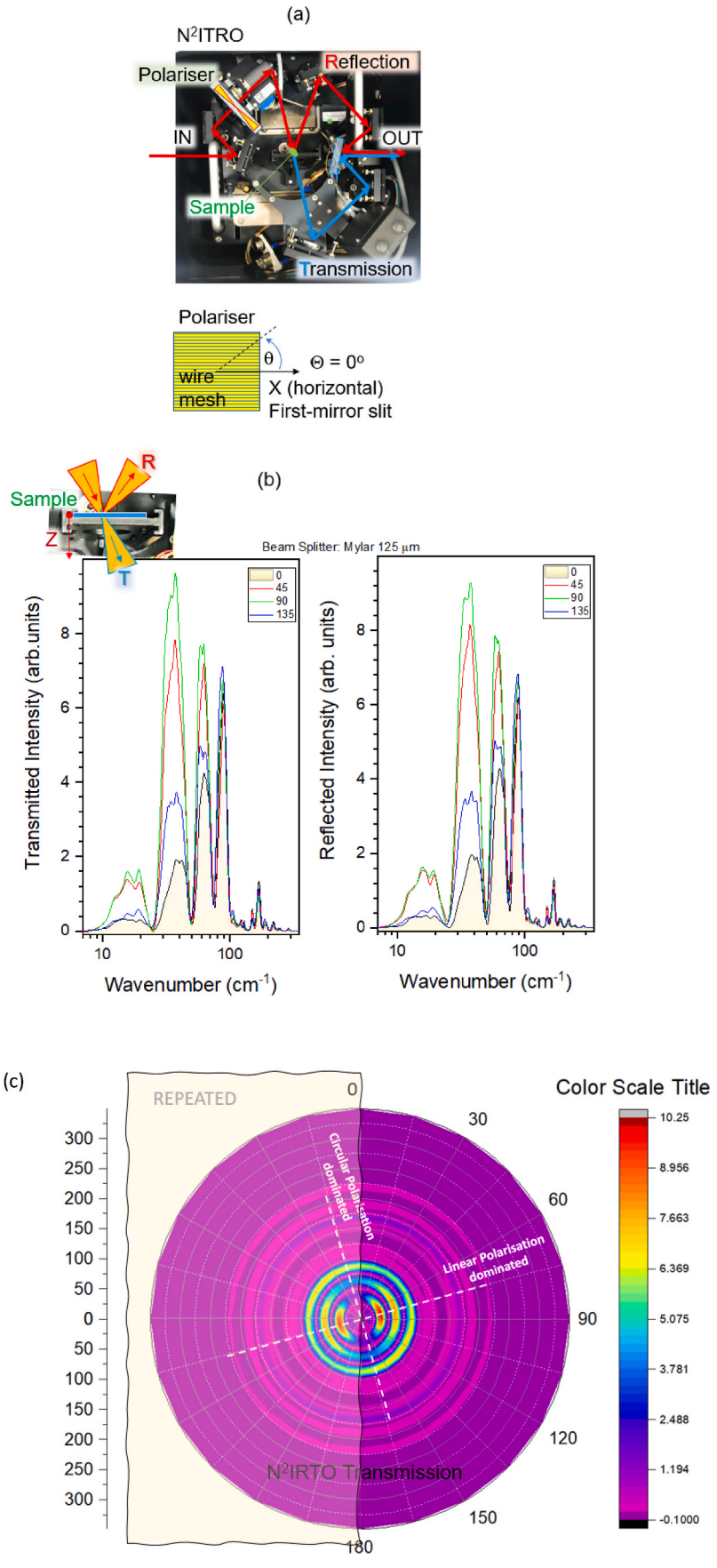

(caption on next page)

Fig. 9. (a) Photo of the near-normal incidence transmission-reflection (N2ITRO, Bruker) unit used in this study with wire-mesh polariser. (b) Intensity in transmission I_T (no sample) and reflection I_R (Au mirror) measured at four orientation angles of polariser θ. (c) Angular dependence of narrow THz radiation with the beamsplitter Mylar 125 μm measured in transmission modes; inset shows sample holder which was moved along z-axis to match sample and Au-mirror positions. The beam splitter was a Mylar 125 μm film and a liquid nitrogen cooled Si bolometer was used as a detector.

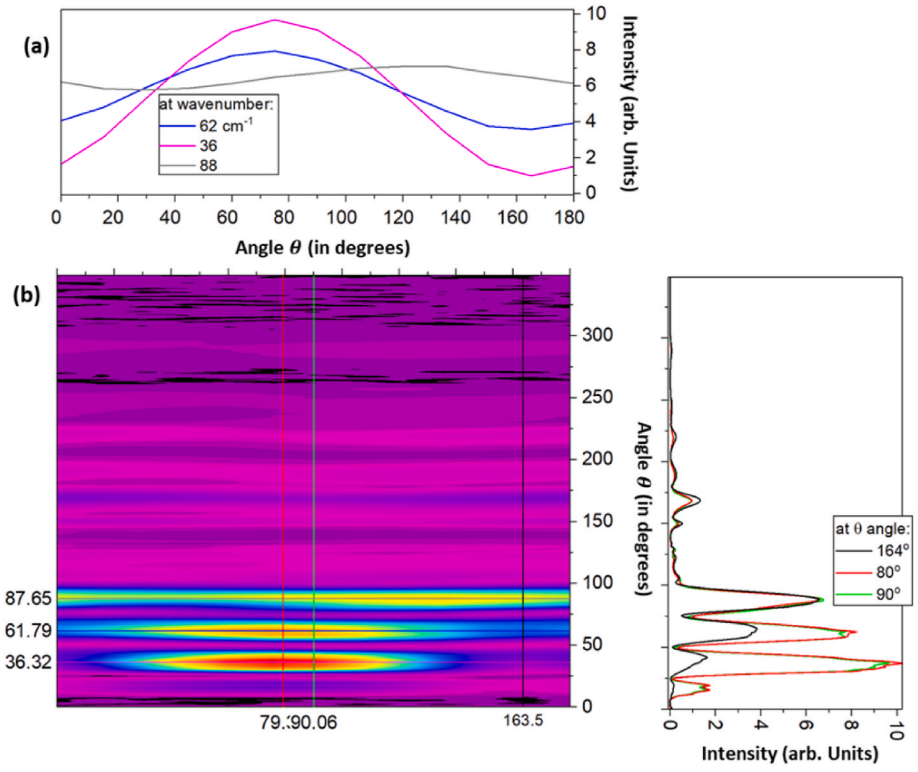

Fig. 10. (a) Orientation dependence of synchrotron radiation (transmission); (b) Spectrum-polarization map of THz synchrotron radiation.

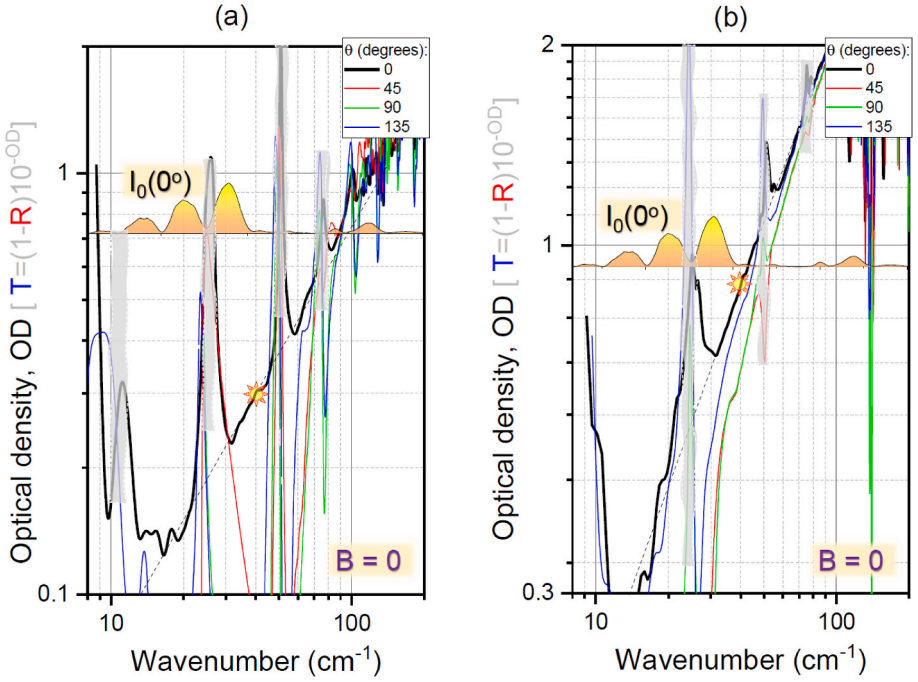

Fig. 11. Optical density of (a) PVA film and (b) PVA-Graphene composite film (5 wt% PVA -1 wt% Graphene). The films were cured in the absence of magnetic field, hence B = 0 T. The spectral profile of the synchrotron with Mylar 125 μm beam splitter is shown as $I_0(0^0)$. The dashed line shows the slope = 1.

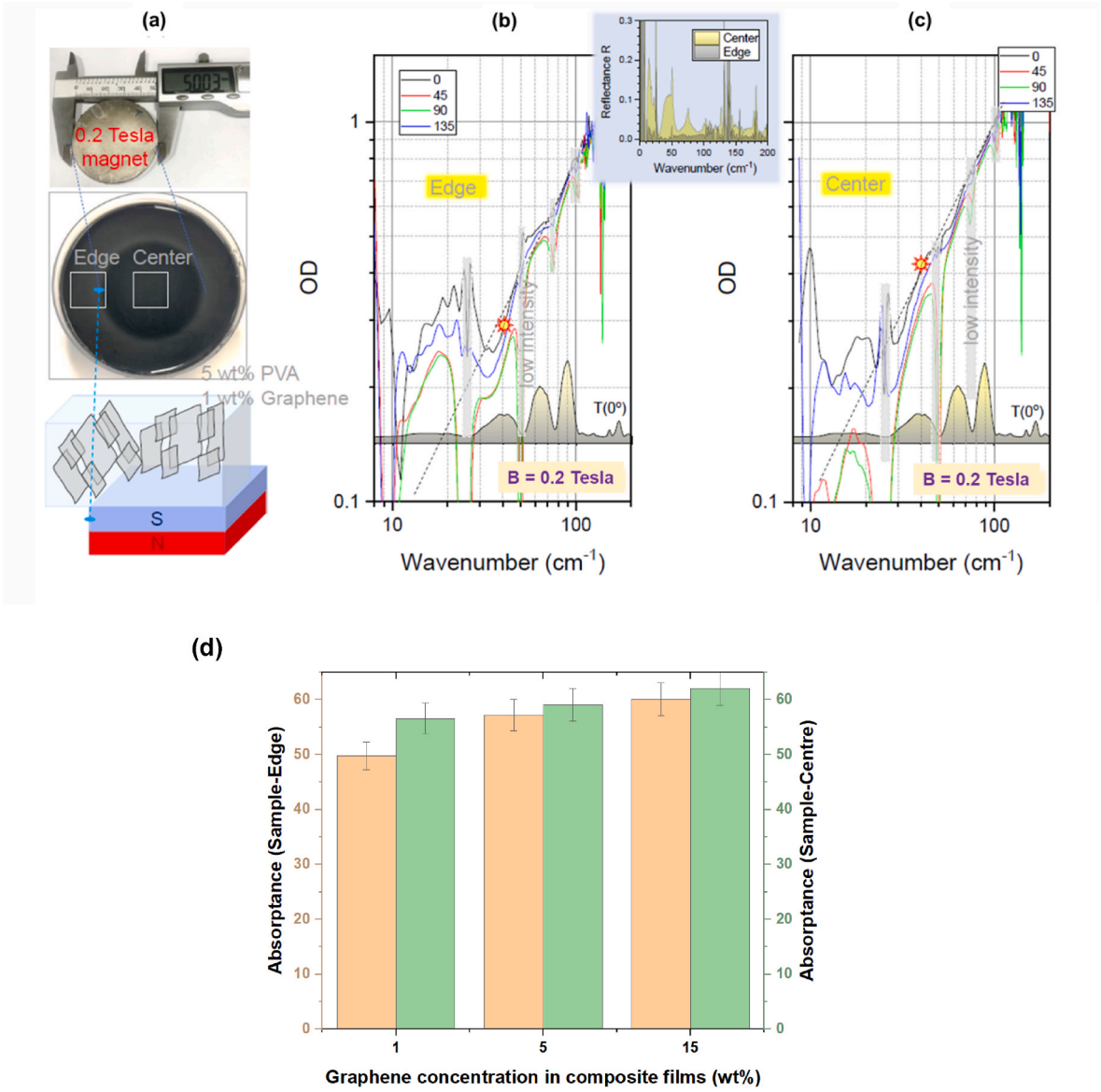

Fig. 12. (a) PVA-Graphene composite (5 wt%-1wt%) made on B = 0.2 T magnet. Absorbance spectra OD ($\widetilde{\nu}$) from the sample edge (b) and sample center (c) regions at different polarisations θ. The inset shows reflectivity spectra at θ = 0°. The star-markers are at $\widetilde{\nu} = 40$ cm^{-1}.

Dopants such as nitrogen and boron, modified the electronic properties of graphene, increasing free charge density and thereby enhancing the absorption efficiency. Creating structural defects in graphene through plasma treatment and ion irradiation enhances the density of interaction sites, thereby improving THz wave absorption. Engineering graphene is regarded as a more efficient approach than relying on high graphene concentrations or strong magnetic fields.

4. Conclusions

We report a facile approach to align graphene flakes in composite films using static external magnetic field. The composite films were systematically characterised to understand the mechanism of alignment, quantify the alignment and the enhancement in properties: electrical and optical. Facile fabrication of aligned graphene composite films (concentrations: 1, 5, 10 and 15 wt%) were successfully fabricated using static low magnetic field strength of 0.2 T and curved in oven at 80 °C. The alignment of graphene in the composite film was observed as bright and dark region in the film. However, this pattern was not observed when the graphene concentration was higher than 10 wt%. SEM confirms the orientation of graphene along the magnetic lines of force in the films. The cross-sectional view of the films also verifies the vertical orientation of graphene flakes inside the film. The morphological study also shows the chain-like structure of the graphene in the aligned composite films. Graphene being a strong diamagnetic material, without any chemical modifications were able to orient in polymer solution in the presence of static magnetic field. Graphene is modelled as an ellipsoidal disc and mathematical expressions for magnetic moment of graphene flakes in magnetic field was derived. Further during the orientation, the graphene flakes experience magnetic and potential energies. The magnetic potential energy of graphene flakes is maximum at $\theta = 90^o$ and minimum at $\theta = 0^o$ the gravitational energy is maximum when the in-plane axis of graphene lies parallel to the horizontal surface (i.e. $\theta = 0^o$) and minimum when flakes are oriented vertically (i.e. $\theta = 90^o$). As the magnetic field increases from 0.1 to 1T, the magnetic potential energy becomes dominated which signifies the out-of-plane alignment. It is observed that the orientation of graphene flakes remains independent of the temperature (10, 25 and 80°C) by estimating the probability of alignment of graphene flakes at different magnetic field. SANS study was carried out to visualise and quantify the alignment

of graphene in polymer solutions. The *in-situ* study confirms the anisotropic 2D scattering pattern arising due to the alignment of graphene. Further, the effect of concentration and temperature of the alignment of graphene was investigated and the alignment is quantified in each case by estimating the scattering anisotropy factor - $A(q)$. From the $A(q)$ values, we can confirm the applied magnetic field can only orient the graphene flakes and orientation angle θ is not always 90°. In fact, the results obtained in SANS study complements the theoretical study. The properties enhancement in aligned composite films were characterised for electrical and optical properties. At room temperature, for a filler content of 15 wt%, the electrical conductivity of aligned PVA-graphene film is 1.78 x 10^{-5} S/cm and for randomly distribute PVA-graphene film is 2.82 x 10^{-7} S/cm was observed. It can be concluded that alignment of graphene using magnetic field aided in enhanced mobility and more conducting channels compared to randomly distributed composite films with many insulating gaps (low electrical permeability) and poor dispersion. For the first time, the aligned PVA-Graphene composite films were characterised using THz spectroscopy to understand the optical properties in lowest wavenumbers 10–100 cm^{-1} region. Maximum of 56.6 % of the incident THz radiation was absorbed by the aligned composite consisting of just 1 wt% graphene. The origin of stronger absorbance is related to the THz electrical near-field localisation inside the region of low refractive index, the flake, with dominant E-field component perpendicular to the surface of graphene flake. E-field in such region is in p-pol. orientation and is stronger absorbed. Thus, alignment of graphene flakes significantly improved the electrical and optical properties of the composites. Since our composites are thin films, they find potential applications in packaging of electronics and coatings. Engineering of 3D metamaterials with tailored electric and magnetic properties using externally applied magnetic fields has now a new instrument in the toolbox.

CRediT authorship contribution statement

Premika Govindaraj: Visualization, Methodology, Conceptualization, Formal analysis, Writing – review & editing, Writing – original draft, Validation, Investigation. **Sleeba Varghese:** Writing – review & editing, Methodology, Formal analysis. **Anna Sokolova:** Software, Visualization, Formal analysis, Writing – review & editing, Validation. **Molong Han:** Formal analysis, Writing – review & editing, Fuß Franz Konstantin: Investigation, Writing – review & editing, Supervision. **Saulius Juodkazis:** Validation, Writing – review & editing, Formal analysis. **Dominique Appadoo:** Formal analysis, Methodology, Writing – review & editing. **Franz Konstantin Fuss:** Formal analysis, Writing – review & editing, Supervision, Investigation. **Nisa Salim:** Validation, Resources, Writing – review & editing, Investigation, Data curation. **Nishar Hameed:** Writing – review & editing, Project administration, Conceptualization, Supervision, Funding acquisition.

Declaration of competing interest

The authors declare the following financial interests/personal relationships which may be considered as potential competing interests: NA.

Acknowledgements

Author PG would also like to acknowledge the Swinburne University Postgraduate Research Awards research grant and thank AINSE Limited for providing financial assistance (PGRA - ALNSTU12654). This research was undertaken on the Bilby – time-of-flight small angle neutron scattering instrument (Proposal number - DB9588, *In-situ* SANS analysis of magnetic field induced orientation of graphene flakes in polymer dispersions at different temperatures) at ANSTO and THz-Far IR beamline (Proposal number - 17675, 17675b, Terahertz (THz) conductivity of graphene composite films with random and aligned morphology) at Australian Synchrotron. The authors would like to thank the Australian Research Council for the ARC Linkage Project (LP200301659) research grant.

Appendix A. Supplementary data

Supplementary data to this article can be found online at https://doi.org/10.1016/j.compositesb.2025.112739.

Data availability

No data was used for the research described in the article.

References

[1] Huang H-h, Juodkazis S, Gamaly EG, Nagashima T, Yonezawa T, Hatanaka K. Spatio-temporal control of THz emission. Commun Phys 2022;5:134.
[2] Zhang J, Li S, Le W. Advances of terahertz technology in neuroscience: current status and a future perspective. iScience 2021;24.
[3] Iwaszczuk K, Jepsen P, Heiselberg H. Terahertz technology for defense and security-related applications, vol.172. Technical University of Denmark; 2012.
[4] Shafie A, Yang N, Han C, Jornet JM, Juntti M, Kurner T. Terahertz communications for 6G and beyond wireless networks: challenges, key advancements, and opportunities. IEEE Network 2022;37:162–9.
[5] Govindaraj P, Fox B, Aitchison P, Hameed N. A review on graphene polymer nanocomposites in harsh operating conditions. Ind Eng Chem Res 2019;58:17106–29.
[6] Govindaraj P, Sokolova A, Salim N, Juodkazis S, Fuss FK, Fox B, Hameed N. Distribution states of graphene in polymer nanocomposites: a review. Compos B Eng 2021;226:109353.
[7] Anderson L, Govindaraj P, Ang A, Mirabedini A, Hameed N. Modelling, fabrication and characterization of graphene/polymer nanocomposites for electromagnetic interference shielding applications. Carbon Trends 2021;4:100047.
[8] Saini P, Arora M. Microwave absorption and EMI shielding behavior of nanocomposites based on intrinsically conducting polymers, graphene and carbon nanotubes. New polymers for special applications 2012;3:73–112.
[9] Shakir MF, Khan AN, Khan R, Javed S, Tariq A, Azeem M, Riaz A, Shafqat A, Cheema HM, Akram MA. EMI shielding properties of polymer blends with inclusion of graphene nano platelets. Results Phys 2019;14:102365.
[10] Barani Z, Kargar F, Godziszewski K, Rehman A, Yashchyshyn Y, Rumyantsev S, Cywiński G, Knap W, Balandin AA. Graphene epoxy-based composites as efficient electromagnetic absorbers in the extremely high-frequency band. ACS applied materials & interfaces 2020;12:28635–44.
[11] Sokolova A, Whitten AE, de Campo L, Christoforidis J, Eltobaji A, Barnes J, Darmann F, Berry A. Performance and characteristics of the BILBY time-of-flight small-angle neutron scattering instrument. J Appl Crystallogr 2019;52:1–12.
[12] Steinert BW, Dean DR. Magnetic field alignment and electrical properties of solution cast PET–Carbon nanotube composite films. Polymer 2009;50:898–904.
[13] Camponeschi E, Vance R, Al-Haik M, Garmestani H, Tannenbaum R. Properties of carbon nanotube–polymer composites aligned in a magnetic field. Carbon 2007;45:2037–46.
[14] Tian B, Lin W, Zhuang P, Li J, Shih T-m, Cai W. Magnetically-induced alignment of graphene via landau diamagnetism. Carbon 2018;131:66–71.
[15] Nguyen J, Conca DV, Stein J, Bovo L, Howard CA, Llorente Garcia I. Magnetic control of graphitic microparticles in aqueous solutions, vol.116. Proceedings of the National Academy of Sciences; 2019. p. 2425–34.
[16] Jones TB. Electromechanics of particles. Cambridge: Cambridge University Press; 1995.
[17] Erb RM, Libanori R, Rothfuchs N, Studart AR. Composites reinforced in three dimensions by using low magnetic fields. Science 2012;335:199–204.
[18] Guo X, Cheng S, Yan B, Li Y, Zhou Y, Cai W, Zhang Y, Zhang X-a. Extraordinary thermal conductivity of polyvinyl alcohol composite by aligning densified carbon fiber via magnetic field. Nano Res 2023;16:2572–8.
[19] Zákutná D, Graef K, Dresen D, Porcar L, Honecker D, Disch S. In situ magnetorheological SANS setup at institut laue-langevin. Colloid Polym Sci 2021;299:281–8.
[20] Wu S, Ladani RB, Zhang J, Bafekrpour E, Ghorbani K, Mouritz AP, Kinloch AJ, Wang CH. Aligning multilayer graphene flakes with an external electric field to improve multifunctional properties of epoxy nanocomposites. Carbon 2015;94:607–18. %@ 0008-6223.
[21] Das M, Pani TK, Sundaray B. Electrical properties of solution cast films of polystyrene/polyaniline-multiwalled carbon nanotube nanocomposites. Composites Part C: Open Access 2020;2:100025.
[22] Ryu M, Linklater D, Hart W, Balčytis A, Skliutas E, Malinauskas M, Appadoo D, Tan Y-RE, Ivanova EP, Morikawa J. 3D printed polarizing grids for IR-THz synchrotron radiation. J Opt 2018;20:035101.
[23] Li Z-Z, Fan H, Wang L, Zhang X, Zhao X-J, Yu Y-H, Xu Y-S, Wang Y, Wang X-J, Juodkazis S. Super-stealth dicing of transparent solids with nanometric precision. Nat Photonics 2024;18:799–808.